Eur. Phys. J. A **14**, 199–206 (2002)
DOI 10.1140/epja/i2001-10121-4

THE EUROPEAN PHYSICAL JOURNAL A

γ-radiation of excited nuclear discrete levels in peripheral heavy ion collisions

V.L. Korotkikh[a] and K.A. Chikin

Scobeltsyn Institute of Nuclear Physics, Moscow State University, 119899 Moscow, Russia

Received: 14 December 2001
Communicated by by W. Henning

Abstract. A new process of a nuclear excitation to discrete states in peripheral heavy ion collisions is studied. High-energy photons are emitted by the exited nuclei with energies up to a few tens of GeV at angles of a few hundred microradians with respect to the beam direction. We show that a two-stage process, where an electron-positron pair is produced by virtual photons emitted by nuclei and then the electron or positron excites the nucleus, has a large cross-section. It is equal to about 5 b for CaCa collisions. On the one hand, it produces a significant γ-rays background in the nuclear fragmentation region but, on the other hand, it could be used for monitoring the nuclear beam intensity at the LHC. These secondary nuclear photons could be a good signal for triggering peripheral nuclear collisions.

PACS. 25.75.-q Relativistic heavy ion collisions

1 Introduction

Two-photon physics calls for attention. It includes the effects of coherent photon interactions for nuclear peripheral collisions. Such processes take place at large distances between nuclei, $b > 2R_A$, where b is the impact parameter. The interactions are therefore due to long-range electromagnetic processes. The cross-section is proportional to $(\alpha Z)^4$ for $Z_1 = Z_2 = Z$, where Z is the charge of each ion A_Z. The ions are on essentially undisturbed and fly in the beam direction.

There are many theoretical studies of two-virtual-photon fusion to a particle of mass M in peripheral AA collisions:

$$\gamma^* + \gamma^* \to M. \tag{1}$$

Photons fusion can produce particles from $\mu^{\pm}$, $\tau^{\pm}$ leptons to Higgs bosons [1–5]. Research in this field can yield fundamental results. A full list of references can be found in the recent reviews [1–3].

We considered three competitive processes in our previous work [5] in which π^0-mesons are produced in peripheral AA collisions. The virtual-photon fusion,

$$\gamma^* + \gamma^* \to \pi^0\,, \tag{2}$$

can give π^0-mesons in the central rapidity region and at $p_{\rm T}$ less than 75 MeV. The photodisintegration of a nucleus,

$$\gamma^* + A_Z \to \pi^0 + X\,, \tag{3}$$

also produces π^0-mesons with large amount of nuclear fragments in the fragmentation region [6,7]. Hadronic interactions in the tails of the nuclear density at $b > 2R_A$,

$$A_Z + A_Z \to \pi^0 + X\,, \tag{4}$$

produces π^0's in the whole rapidity region together with the nuclear fragments and other particles in the fragmentation region. We demonstrated [5] that, to distinguish the fusion process (2) from processes (3) and (4), it is necessary to choose a strong $p_{\rm T}$ cut, $p_{\rm T} < 75$ MeV, for all produced particles. Additionally it is necessary to have an efficient trigger to distinguish photon-photon events from hadronic ones. G. Baur *et al.* [3] suggested to measure intact nuclei after the interaction. Evidently this is impossible in the CMS. The nuclei at such low $p_{\rm T}$ will emit in a very small solid angle, $\theta_A \leq 1$ μrad, at LHC energies and fly into the beam pipe. We are interested in the fusion process (2) where both nuclei preserve their A and Z. It is the necessary to remove the contributions in eqs. (3) and (4) by the help of the veto-detectors on nuclear fragments.

The separation of peripheral and central AA collisions is a hard experimental problem. There are two suggestions to select peripheral events: the correlation between b and the total transverse energy $E_{\rm T}$ [8] or the correlation of b and particle multiplicity [9]. But there are no "event-by-event" criteria for peripheral collision selection.

The two-photon fusion (1) is accompanied by other electromagnetic processes which have to be considered if we want to obtain a clear signature of the process (1).

The pure electromagnetic processes of the electron-positron pair production [10–13] and bremsstrahlung pho-

[a] e-mail: vlk@lav01.sinp.msu.ru

tons [14–17] are also studied. These processes are considered as a possible background contribution. The cross-section of the e^+e^- pair production is huge, 220 Kb for PbPb and 1.5 Kb for CaCa collisions at LHC energies. We will use the fact of the huge e^+e^- cross-section below.

The physical program of LHC heavy ions includes the nuclei Pb, Nb, Ar and O. Our calculations for CaCa are close to those for ArAr collisions. We choose Ca because this nucleus is studied very well, the electromagnetic form factors are well known from experiments. We have no free parameters in our calculations.

The direct bremsstrahlung from the heavy ion,

$$A_Z + A_Z \to A_Z + A_Z + \gamma'_{\rm BS}\,, \tag{5}$$

is small [14–16] with a cross-section proportional to $Z^6\alpha^3/M_A^2$. In ref. [17] it is suggested to measure the bremsstrahlung photons coming from electrons and positrons produced in peripheral ion collisions,

$$A_Z + A_Z \to A_Z + A_Z + e^+e^- + \gamma'_{\rm BS}\,. \tag{6}$$

The cross-section is proportional to $Z^4\alpha^5/m_e^2$, and it is larger than the cross-section of process (5). We used the result of ref. [17] for PbPb and found about 10 b for CaCa at LHC energies. The energies of bremsstrahlung photons are small, $E_{\gamma'_{\rm BS}} \leq 3$ MeV, and the angles are near $\theta_{\gamma'_{\rm BS}} = 1^\circ$. Such low-energy photons are impossible to measure. So they are not a good signature of peripheral AA collisions.

In the present work we study a new process in which a nucleus is excited to discrete levels by an electron (positron) produced in electromagnetic interaction between nuclei:

$$A_Z + A_Z \to A_Z^* + A_Z + e^+e^-\,. \tag{7}$$

The excited nucleus A_Z^* radiates the secondary photon γ':

$$A_Z^* \to A_Z + \gamma'\,. \tag{8}$$

As a rule, the nuclear excitation energy is a few MeV [18]. The energies $E^0_{\gamma'}$ of the photon in the nucleus rest system are in MeV scale. They will be equal to about 10 GeV or more in the laboratory system at LHC energies. The polar angle $\theta_{\gamma'}$ of the secondary photon is about a few hundred μrad. It allows favourable conditions for the photon measurement and using the secondary photons as a trigger for peripheral collisions. The process (8) was suggested as a possible explanation of the high-energy ($E_\gamma \geq 10^{12}$ eV) cosmic photon spectrum [19].

There are other processes which could produce secondary photons. Mesons are produced by the fusion process (1) and decay to photons as $\pi^0 \to 2\gamma$. Neutral pions can also be produced by double Pomeron (IP) exchange [20] in AA collisions,

$$\mathrm{IP} + \mathrm{IP} \to \pi^0 + \mathrm{X}\,. \tag{9}$$

The calculations of the PHOJET event generator [21] for Pomeron exchange give an average transverse momentum of about 450 MeV for pions. The calculations in ref. [22] show that the cross-section of the double Pomeron (IP) exchange is smaller than the fusion process (1) for heavy ions and is comparable for medium nuclei.

There are other competitive processes which also produced secondary photons. Such as nuclear excitation,

$$A_Z + A_Z \to A_Z^* + A_Z, \qquad A_Z^* \to \gamma' + A_Z, \tag{10}$$

in peripheral collisions at $b > 2R$. We will show that the cross-section is smaller than process (7). It is also possible to excite one nucleus by a virtual photon from another nucleus,

$$\gamma^* + A_Z \to A_Z^*, \qquad A_Z^* \to \gamma' + A_Z. \tag{11}$$

The cross-section of this process is the same as or smaller than (10) for intermediate-mass ions with $Z_A \approx 20$.

Other processes which are also a source of secondary photons are the excitation of nuclei to the continuum with cascade transitions to lower nuclear states that emit photons. Such processes have a large probability to decay, $A^* \to (A-4) + {}^4\mathrm{He}$, $A^* \to (A-1) + \mathrm{N}$, if the excitation energy is higher than the particle decay threshold [18]. It might be possible to remove these decays by vetoing charged particles. We also need to exclude the secondary-photon contribution from nuclear fragments in photodisintegration reactions:

$$\gamma^* + A_Z \to A_1^* + A_2^* + \ldots, \qquad A_k^* \to \gamma + A_k\,. \tag{12}$$

Our estimates, based on ref. [6] using RELDIS, show that the nuclear fragments scatter in small angles $\theta \leq 45$ μrad. These fragments do not hit the central detectors but can be removed either by the quadruple lens or by the Roman pots of TOTEM [23].

The TOTEM detector will measure protons at small t, $0.02 < |t| < 0.7$ $(\mathrm{GeV/c})^2$, corresponding to small polar angles, $20 < \theta < 120$ μrad, with respect to the beam direction. We will show that the cross-section of (7) is large, $\sigma \approx 5$ barn, so that secondary photons hit the Roman pots with high rates and can be a significant background, resulting in the degradation of the detector.

There are two ways to use the secondary photons produced by process (7). One possibility is to use them for monitoring the nuclear-beam intensity. At RHIC a neutron zero-degree calorimeter (ZDC) [24] is used. The beam-crossing angle at RHIC is 14 mrad and the ZDC measures neutrons in the region $\Delta\theta = 6$ mrad. The LHC beam-crossing angle is very small, 300 μrad. As yet, a nuclear-beam intensity monitor has not developed. The possibility of using (7) to monitor the nuclear beam at LHC is important.

The second application concerns triggering peripheral nucleus-nucleus collisions in processes as

$$A_Z A_Z \to A_Z^* A_Z + e^+e^- + M\,, \quad A_Z^* \to \gamma' + A_Z\,; \tag{13}$$

$$A_Z A_Z \to A_Z^* A_Z + M\,, \quad A_Z^* \to \gamma' + A_Z\,, \tag{14}$$

where M is the produced particle system. The total trigger requirements include the following features: a signal in the central rapidity region from $\gamma^*\gamma^* \to M$ events, the

absence of charged particles in the nuclear fragmentation region and a photon signal in the Roman pots. We do not calculate these processes here, but study the angular and energy distributions of secondary photons in decay (8) for process (7). Note that these distributions should be similar to those of processes (13) and (14).

2 Formalism

2.1 Secondary nuclear γ-radiation

We study the photon radiation of the relativistic nucleus from the discrete level

$$A^*(J^P, E_\gamma^0) \to A + \gamma'. \tag{15}$$

The secondary photon γ' flies off at an angle $\theta_\gamma{}'$ and at an energy E_γ^0 in the nucleus rest (NR) system. If a nucleus has Lorenz factor γ_A, then the secondary-photon energy is

$$E_\gamma = \gamma_A E_\gamma^0 (1 + \cos\theta_\gamma{}') \tag{16}$$

in the laboratory system (LS), so that $0 \le E_\gamma \le 2\gamma_A E_\gamma^0$ and

$$\left|\frac{\mathrm{d}E_\gamma}{\mathrm{d}\theta_\gamma{}'}\right| = \gamma_A E_\gamma^0 \ \sin\theta_\gamma{}'. \tag{17}$$

The angles in the LS and the NR systems are related by

$$\tan\theta_\gamma = \frac{1}{\gamma_A}\frac{\sin\theta_\gamma{}'}{(1+\cos\theta_\gamma{}')}. \tag{18}$$

Then

$$\frac{\mathrm{d}\theta_\gamma{}'}{\mathrm{d}\theta_\gamma} = \frac{2\gamma_A}{(1+\gamma_A^2\tan^2\theta_\gamma)\cos^2\theta_\gamma}. \tag{19}$$

Photon number conservation gives

$$f(E_\gamma)\mathrm{d}E_\gamma = f(\theta_\gamma{}')\mathrm{d}\theta_\gamma{}'. \tag{20}$$

The angular and energy distributions of the secondary photons in the LS are

$$\frac{\mathrm{d}P_{A^*}(\theta_\gamma)}{\mathrm{d}\theta_\gamma} = f(\theta_\gamma{}')\frac{\mathrm{d}\theta_\gamma{}'}{\mathrm{d}\theta_\gamma}, \tag{21}$$

$$\frac{\mathrm{d}P_{A^*}(E_\gamma)}{\mathrm{d}E_\gamma} = f(\theta_\gamma{}')\frac{\mathrm{d}\theta_\gamma{}'}{\mathrm{d}E_\gamma} = f(\theta_\gamma{}')\frac{\Theta(2\gamma_A E_\gamma^0 - E_\gamma)}{\gamma_A E_\gamma^0 \sin\theta_\gamma{}'}, \tag{22}$$

where $\Theta(x) = 1$, if $x \le 0$ and $\Theta(x) = 0$, if $x > 0$.

For an isotropic photon distribution in the NR system

$$f(\theta_\gamma{}')\mathrm{d}\theta_\gamma{}'\mathrm{d}\varphi_\gamma{}' = \frac{1}{4\pi}\sin\theta_\gamma{}'\mathrm{d}\theta_\gamma{}'\mathrm{d}\varphi_\gamma{}'. \tag{23}$$

After integration over $\varphi_\gamma{}'$, we have

$$\frac{\mathrm{d}P_{A^*}(\theta_\gamma)}{\mathrm{d}\theta_\gamma} = \frac{1}{2}\frac{\sin\theta_\gamma{}'\ \mathrm{d}\theta_\gamma{}'}{\mathrm{d}\theta_\gamma}, \tag{24}$$

$$\frac{\mathrm{d}P_{A^*}(E_\gamma)}{\mathrm{d}E_\gamma} = \frac{1}{2\gamma_A E_\gamma^0}\Theta(2\gamma_A E_\gamma^0 - E_\gamma). \tag{25}$$

For comparison the photon distribution of the π^0 decay is

$$\frac{\mathrm{d}P_{\pi^0}(E_\gamma)}{\mathrm{d}E_\gamma} = \frac{1}{\gamma_{\pi^0} m_{\pi^0}}\Theta(\gamma_{\pi^0} m_{\pi^0} - E_\gamma). \tag{26}$$

The angular photon distribution (24) is

$$\frac{\mathrm{d}P_{A^*}}{\mathrm{d}\theta_\gamma} = \frac{2\ \gamma_A^2\ \sin\theta_\gamma}{(1+\gamma_A^2\tan^2\theta_\gamma)^2\cos^3\theta_\gamma} \tag{27}$$

in the LS.

2.2 Excitation of the discrete nuclear level in quasi-elastic electron scattering

We follow the formalism of ref. [25]. The cross-section for the nuclear excitation by electron scattering

$$e + A \to e' + A^*(\lambda^P, E_\gamma^0) \tag{28}$$

is

$$\frac{\mathrm{d}\sigma_{A^*}}{\mathrm{d}\Omega'} = \sigma_{\mathrm{M}}(q) F_\lambda^2(q). \tag{29}$$

Here we neglect the nuclear recoil effect. The equation is valid in the NR system where the electron has an energy ε_0 and the momentum transfer is

$$q = 2\varepsilon_0 \sin\frac{\Theta_{e'}}{2}, \tag{30}$$

where $\Theta_{e'}$ is a scattering angle of the electron. The Mott cross-section of the electron scattering off charge Z_A is

$$\sigma_{\mathrm{M}}(q) = \left(\frac{2\ Z_A e^2}{q^2}\ \varepsilon_0\cos(\theta_{e'}/2)\right)^2 = \frac{\alpha^2 Z_A^2\ \cos^2(\theta_{e'}/2)}{(2\varepsilon_0\sin^2(\theta_{e'}/2))^2}. \tag{31}$$

Here $\hbar = c = 1$.

A good approximation of the measured inelastic form factor $F_\lambda(q)$ [25] is

$$F_\lambda(q) = \frac{c_\lambda q^\lambda}{Z_A}\left[1 - \beta\left(\lambda + \frac{3}{2}\right) + \frac{\beta}{4}(dq)^2\right]e^{-(dq)^2/4} \tag{32}$$

$$c_\lambda = \frac{N_\lambda \pi\sqrt{2\lambda+1}\, d^{\lambda+3}}{2^{\lambda+1}}. \tag{33}$$

The parameters for $^{40}\mathrm{Ca}^*(3^-, 3.74\ \mathrm{MeV})$ are $\lambda = 3$, $N_3 = 0.0496\ \mathrm{fm}^{-3}$, $d = 2.015$ fm and $\beta = 0.8$.

The four-momenta of the electron and nucleus are

$$\begin{aligned} k_e &= (\varepsilon, p\sin\theta\ \cos\varphi, p\sin\theta\ \sin\varphi, p\cos\theta), \\ k_A &= (E_A, 0, 0, -p_A) \end{aligned} \tag{34}$$

in the laboratory system and

$$k_e{}' = (\varepsilon_0, \mathbf{p}_e{}'), k_A{}' = (m_A, 0) \tag{35}$$

in the nuclear rest system.

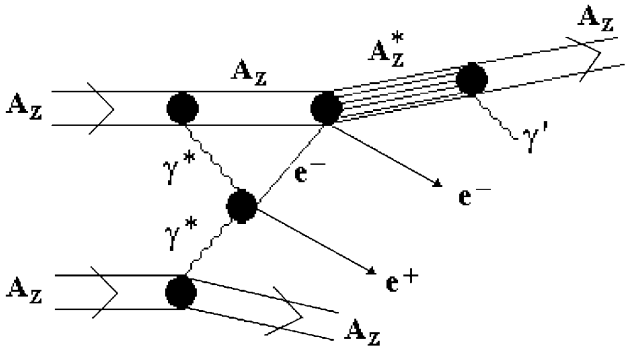

Fig. 1. Diagram of the two-stage process of nuclear excitation by an electron (positron) produced by the virtual-photon interaction in an AA collision at the LHC.

Then

$$\varepsilon_0 = \frac{1}{m_A}(\varepsilon E_A + p\ p_A \cos\theta), \tag{36}$$

$$q_{\max}(\varepsilon_0) = 2\ \varepsilon_0, \tag{37}$$

where θ is the polar angle of the electron in the LS with the z-axis parallel to $\mathbf{p}_A$, the nuclear momentum.

Equations (36), (37) allows us to calculate the cross-section of the quasi-elastic excitation electron scattering in the system of the colliding nuclei.

2.3 Nuclear excitation by electron or positron in peripheral heavy ion collisions

In fig. 1 we show the two-stage process

$$A_Z + A_Z \to A_Z^* + A_Z + e^+e^-, \tag{38}$$

where the e^+e^- pair is produced by the virtual photons in the nuclear electromagnetic field followed by nuclear excitation by the electron or positron.

The authors of ref. [10] showed that the energy and angular electron (positron) distribution in the double equivalent photon approximation is

$$\frac{\mathrm{d}\sigma_{AA}}{\mathrm{d}\varepsilon\mathrm{d}\Omega} = \frac{\alpha^2}{2} p \int\limits_{\hat{E}/2}^{\infty} \frac{\mathrm{d}\omega}{\omega^4} \frac{2\omega - \hat{E}}{\tilde{E}^2} n(\omega) n\left(\frac{\omega\hat{E}}{2\omega - \tilde{E}}\right)\ g(\omega,\theta)\,, \tag{39}$$

where ω is the energy of the virtual photon. We have

$$\begin{aligned} \hat{E} &= \varepsilon + p\cos\theta, \\ \tilde{E} &= \varepsilon - p\cos\theta, \\ \varepsilon^2 &= p^2 + m_e^2, \end{aligned} \tag{40}$$

$$g(\omega,\theta) = \left\{ \frac{2\omega\omega' - m_e^2 + (\omega\omega' - m_e^2)\sin^2\theta}{m_e^2 - (\omega\omega' - m_e^2)\sin^2\theta} - \frac{2(\omega\omega' - m_e^2)^2 \sin^4\theta}{[m_e^2 + (\omega\omega' - m_e^2)\sin^2\theta]^2} \right\}, \tag{41}$$

$$\omega' = \frac{\omega\tilde{E}}{2\omega - \hat{E}}, \tag{42}$$

$$n(\omega) = \frac{2}{\pi} Z_A^2 \alpha \left(\frac{c}{v}\right)^2 \times \left[\xi K_0(\xi) K_1(\xi) - \frac{v^2\xi^2}{2c^2}(K_1^2(\xi) - K_0^2(\xi))\right], \tag{43}$$

$$\xi = \frac{\omega R_{\min}}{\gamma v}. \tag{44}$$

The equivalent electron approximation [3] is more exact, but the results of that approach are not numerically different from [10].

We consider a model of the two independent simultaneous processes in fig. 1. The cross-section of the two-stage process (38) is written as a convolution of eq. (39) with the probability of nuclear excitation:

$$\sigma_{AA^*} = \int \mathrm{d}\varepsilon\mathrm{d}\Omega\mathrm{d}\Omega' \frac{\mathrm{d}\sigma_{AA}}{\mathrm{d}\varepsilon\mathrm{d}\Omega}(\varepsilon,\theta)\ P_{A^*}(q(\theta';\varepsilon,\theta)). \tag{45}$$

We define the probability of nuclear excitation $P_{A^*}(q)$ as a ratio of the cross-section (29) to the sum over all nuclear final states:

$$P_{A^*}(q) = \frac{\mathrm{d}\sigma_{A^*}/\mathrm{d}\Omega'}{\mathrm{d}\sigma_{\mathrm{sum}}/\mathrm{d}\Omega'}. \tag{46}$$

We follow the Glauber model [26] to calculate this sum using the property of closure. For the electron scattering, we find

$$\frac{\mathrm{d}\sigma_{\mathrm{sum}}}{\mathrm{d}\Omega'} = [Z_A(Z_A - 1)\ S_A^2(q) + Z_A]\ |f_{ep}(q)|^2\,, \tag{47}$$

where $f_{ep}(q)$ is the elastic electron-proton scattering amplitude and $S_A(q)$ is the elastic nuclear form factor. For our two-stage peripheral process where $q \ll 1/R_A$, $S_A(q) \approx 1$, so that

$$\frac{\mathrm{d}\sigma_{\mathrm{sum}}}{\mathrm{d}\Omega'}(q) \approx Z_A^2\ |f_{ep}(q)|^2 = \sigma_{\mathrm{M}}(q). \tag{48}$$

Thus the integrated cross-section, eq. (45), is

$$\sigma_{AA^*} = \int \mathrm{d}\varepsilon\mathrm{d}\Omega\mathrm{d}\Omega' \frac{\mathrm{d}\sigma_{AA}}{\mathrm{d}\varepsilon\mathrm{d}\Omega}(\varepsilon,\theta) F_\lambda^2(q(\theta';\varepsilon,\theta)) = 2\pi^2\ \alpha^2 \int\limits_{\hat{E}/2}^{\infty} \mathrm{d}\omega \int\limits_{m_e}^{\infty} \mathrm{d}\varepsilon \int \mathrm{d}\cos\theta \int \mathrm{d}\cos\theta' \times p(\varepsilon) \frac{2\omega - \hat{E}}{\omega^4 \tilde{E}^2} n(\omega) n(\omega') g(\omega,\theta) F_\lambda^2(q(\theta',\varepsilon,\theta)), \tag{49}$$

where q is defined in eq. (30).

After electro-excitation at high energies, the nucleus A_Z^* essentially retains its direction. Then the angular and energy distributions of the secondary photon are

$$\frac{\mathrm{d}\sigma_{AA^*}(\theta_{\gamma'})}{\mathrm{d}\theta_{\gamma'}} = \sigma_{AA}\ \frac{\mathrm{d}P_{A^*}(\theta_{\gamma'})}{\mathrm{d}\theta_{\gamma'}}, \tag{50}$$

$$\frac{\mathrm{d}\sigma_{AA^*}(E_{\gamma'})}{\mathrm{d}E_{\gamma'}} = \sigma_{AA}\ \frac{\mathrm{d}P_{A^*}(E_{\gamma'})}{\mathrm{d}E_{\gamma'}}, \tag{51}$$

where σ_{AA} is given in eq. (49). The functions $\mathrm{d}P_{A^*}/\mathrm{d}\theta_\gamma$ and $\mathrm{d}P_{A^*}/\mathrm{d}E_\gamma$ depend on the angular distribution of γ' in the NR system. For an isotropic γ' distribution they are given by eqs. (24) and (25).

2.4 Nuclear excitation by the peripheral strong interaction

One possible background for process (7) is a strong interaction in which one of the nuclei is excited to a discrete level:

$$A_1 + A_2 \to A_1^* + A_2. \tag{52}$$

We make a rough estimate of the cross-section in peripheral collisions with $b > (R_1 + R_2)$. We write the differential cross-section for the elastic scattering $A_1 + A_2 \to A_1 + A_2$ [27], neglecting distortion effects:

$$\frac{\mathrm{d}\sigma_{A_1A_2}}{\mathrm{d}q^2} = \frac{\mathrm{d}\sigma_{NN}}{\mathrm{d}q^2}(q^2)|A_1A_2S_{A_1}(\mathbf{q})S_{A_2}(-\mathbf{q})|^2. \tag{53}$$

Here $S_A(\mathbf{q})$ is the nuclear form factor, equal to unity at $q = 0$, $S_A(0) = 1$. We can approximate it simply by a Gaussian nuclear density:

$$S_{A_i}(q) = e^{-B_{A_i}q^2/2}. \tag{54}$$

We use the standard form (see [2]) for the nucleon-nucleon scattering cross-section:

$$\frac{\mathrm{d}\sigma_{NN}}{\mathrm{d}q^2}(q^2) = \left|\frac{\sigma_{\mathrm{tot}}(NN)}{4\sqrt{\pi}}e^{-B_Nq^2/2}\right|^2. \tag{55}$$

We calculate the energy of an AA collision at the LHC with $\gamma = 3500$ in the nuclear rest system, where $\gamma_A = 2\gamma^2 - 1$. The energy of an NN collision in the rest system is $E_p = 2.5{\times}10^7$ GeV. We find $\sigma_{\mathrm{tot}}(NN) \approx 100$ mb and $B_{NN} \simeq 20$ GeV^{-2} at LHC energies from a good approximation of $\bar{p}p$ data at $\sqrt{s_{pp}} < 540$ GeV in ref. [28].

For the elastic scattering we can write the form factor $S_A(\mathbf{q})$ as

$$S_A(q) = 2\pi\int_0^\infty b\mathrm{d}bJ_0(qb)T_A(b), \quad T_A(b) = \int_{-\infty}^\infty \mathrm{d}z\rho_A(\mathbf{b},z), \tag{56}$$

where $J_0(qb)$ is a Bessel function and $\rho_A(\mathbf{b},z)$ is the nuclear density. Using eq. (54), $T_A(b)$ is

$$T_A(b) = \frac{1}{2\pi B_A}e^{-b^2/(2B_A)}. \tag{57}$$

Peripheral collisions will correspond to the integral (56) in the region $b > R$:

$$S_A(q,R) = 2\pi\int_R^\infty b\mathrm{d}bJ_0(qb)T_A(b). \tag{58}$$

The amplitude of the proton inelastic scattering with nuclear excitation to a state with spin λ and projection μ in the same approximation is

$$\mathcal{F}_{pA^*}(\mathbf{q}) = A\ f_{NN}(\mathbf{q})G_{\lambda\mu}(\mathbf{q}), \tag{59}$$

where

$$G_{\lambda\mu}(\mathbf{q}) = \int \mathrm{d}^3\mathbf{r}e^{i\mathbf{q}\cdot\mathbf{r}}\rho_{\lambda\mu}(\mathbf{r}). \tag{60}$$

The inelastic nuclear transition density is

$$\rho_{\lambda\mu}(\mathbf{r}) = \frac{1}{A}\langle\lambda\mu|\sum_{j=1}^A\delta(\mathbf{r}-\mathbf{r}_j)|00\rangle. \tag{61}$$

It is simple to show that $F_{\lambda\mu}(q)|_{q\to0} \sim q^\mu$. We define the inelastic nuclear form factor $S^{(\lambda)}_{A^*}(q)$ as

$$(S^{(\lambda)}_{A^*}(q))^2 = \sum_\mu |G_{\lambda\mu}(\mathbf{q})|^2. \tag{62}$$

If we assume that the state with $\mu = \lambda$ is dominant, we can approximate the inelastic form factor $S^{(\lambda)}_{A^*}(q)$ by eq. (32). This form agrees with form factor from inelastic electron scattering [25]. We assume that the charge and nucleon transition densities are the same with a rough estimate. We take the parameters of the inelastic form factor for $^{40}\mathrm{Ca}^*(\lambda\mu)$ from ref. [25] and renormalize the form factor to Z_A/A, so that

$$S^{(\lambda)}_{A^*}(q) = \frac{Z_A}{A}F_\lambda(q). \tag{63}$$

The Fourier transform analogous to eq. (58) is

$$S^{(\lambda)}_{A^*}(q,R) = 2\pi\int_R^\infty b\mathrm{d}bJ_\lambda(qb)T^{(\lambda)}_{A^*}(b), \tag{64}$$

in peripheral collisions with $b > R$, where the function $T^{(\lambda)}_{A^*}(b)$ can be calculated by the inverse Fourier transform from $S^\lambda_{A^*}(q)$ to $T^\lambda_{A^*}(b)$

$$T^{(\lambda)}_{A^*}(b) = \frac{1}{2\pi}\int_0^\infty q\mathrm{d}qJ_\lambda(qb)S^{(\lambda)}_{A^*}(q). \tag{65}$$

We can calculate (65) analytically with the form factor parameterisation in eq. (63). We have

$$T^{(\lambda)}_{A^*}(b) = \frac{1}{A}\frac{c_\lambda}{2}\left[1-\beta\left(\lambda+\frac{3}{2}\right)+\beta\left(\frac{b}{d}\right)^2\right] \times\left(\frac{4}{d^2}\right)\frac{\lambda+2}{2}\left(\frac{b^2}{d^2}\right)^{\lambda/2}e^{-b^2/d^2}. \tag{66}$$

Thus eq. (53) becomes

$$\frac{\mathrm{d}\sigma_{A_1^*A_2}}{\mathrm{d}q^2} = \frac{\mathrm{d}\sigma_{NN}}{\mathrm{d}q^2}(q^2)|A_1A_2S^{(\lambda)}_{A_1^*}(\mathbf{q},R)\ S_{A_2}(-\mathbf{q},R)|^2. \tag{67}$$

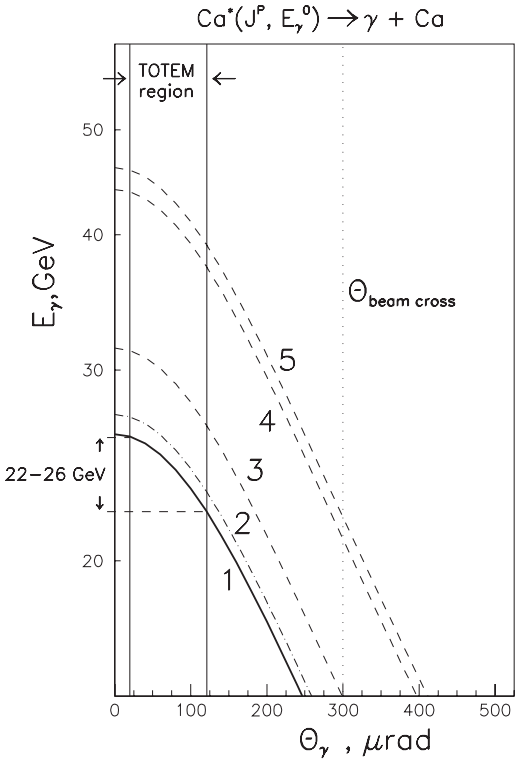

Fig. 2. Energy of photons emitted by $\mathrm{Ca}^*(J^P, E^0_\gamma)$ as a function of the angle. The lines correspond to the discrete excited levels: (1) 3^-_1, 3.74 MeV, (2) 2^+_1, 3.90 MeV, (3) 5^-_1, 4.49 MeV, (4) 3^-_2, 6.29 MeV, (5) 3^-_3, 6.59 MeV. The vertical lines show the TOTEM angular region 20 μrad $\leq \theta <$ 120 μrad and the beam crossing angle.

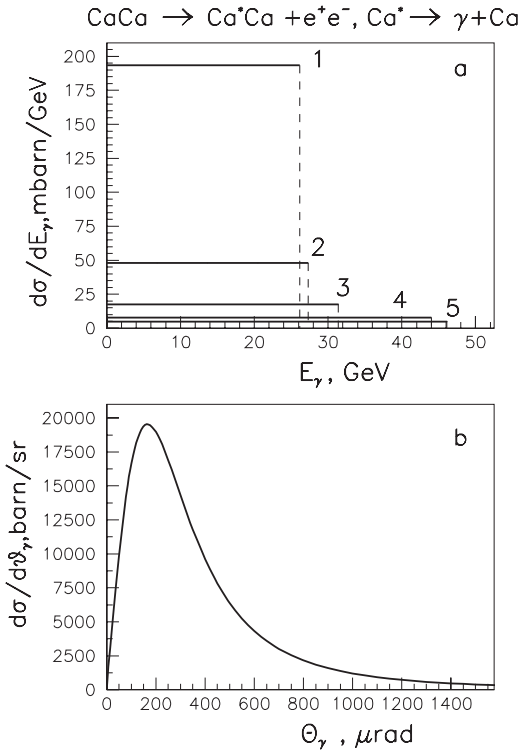

Fig. 3. Energy and angular distributions of secondary photons from $\mathrm{Ca} + \mathrm{Ca} \to \mathrm{Ca}^*(\lambda^P, E^0_\gamma) + \mathrm{Ca} + e^+e^-$, $\mathrm{Ca}^* \to \gamma + \mathrm{Ca}$. (a) Photon energy distributions, numbers 1-5 correspond to the five nuclear levels in fig. 2. (b) Photon angular distribution summed over all levels.

The energy and angular distributions of the secondary photons are given by the convolutions

$$\frac{\mathrm{d}\sigma_{A_1^* A_2}}{\mathrm{d}E_{\gamma_1'}} = \int \mathrm{d}^2 q \frac{\mathrm{d}\sigma_{A_1^* A_2}(q)}{\mathrm{d}q^2} \frac{\mathrm{d}P_{A_1^*}}{\mathrm{d}E_{\gamma_1'}}(E_{\gamma_1'}, \theta_{A_1^*}), \qquad (68)$$

$$\frac{\mathrm{d}\sigma_{A_1^* A_2}}{\mathrm{d}\theta_{\gamma_1'}} = \int \mathrm{d}^2 q \frac{\mathrm{d}\sigma_{A_1^* A_2}(q)}{\mathrm{d}q^2} \frac{\mathrm{d}P_{A_1^*}}{\mathrm{d}\theta_{\gamma_1'}}(|\theta_{\gamma_1'} - \theta_{A_1^*}|). \qquad (69)$$

For symmetric collisions with $A_1 = A_2 = A$ and small angles, $\theta_{A^*} = q/p_A$.

3 Energy and angular distributions of secondary photons

We consider the peripheral processes (2),(7) and (10), which give us the secondary photons. All the three processes preserve the charge Z and nuclear number A of the nucleus. The nucleus is excited and then emits the photons in processes (7) and (10). The π^0-meson produced in process (2) by virtual-photon fusion decays to two photons.

We study the kinematic dependence of E_γ on θ_γ in the LS for ^{40}Ca (see fig. 2). The beam luminosity is $L = (2\text{–}4) \times 10^{30}$ cm^{-2} s^{-1} (see [2]). The characteristics of the Ca discrete level are well known [18]. In fig. 2 we use five strongly excited levels by electrons [25]. The level $\lambda^P = 3^-_1$, $E^0_\gamma = 3.74$ MeV has the largest excitation intensity.

Figure 2 demonstrates that E_γ falls quickly with θ_γ at $\gamma_A = 3500$. The energy is a few tens of GeV in the solid angle $\theta < \theta_{\mathrm{cross}}$. The 3^- excitation gives the secondary photons with energies 22–26 GeV in the angular range of TOTEM.

Figure 3 shows the cross-sections, eqs. (50) and (51), of the two-stage process (7) of the excitation of the nucleus Ca by electron (positron) in the virtual-photon interaction (subsect. 2.3). The angular distribution of the secondary photons in the NR system are assumed to be isotropic because we average over all initial directions of electrons that excite the nucleus (see eq. (24)). The energy distribution in fig. 3a is then uniform. The level 3^-, $E^0_\gamma = 3.74$ MeV gives the largest contribution to the sum of the angle distributions over other levels in fig. 3b. The maximum in the angular distribution is $\theta_\gamma = 150$ μrad.

The integrated cross-section of the two-stage process (7) is equal to $\sigma_1 = 4.8$ b at $R_{\min} = 1/m_e = 386$ fm. The cross-section σ_1 is large because the $\gamma^*\gamma^* \to e^+e^-$ cross-section is rather large, 1.5 Kb for CaCa collisions at LHC energies. In the TOTEM angular region, the cross-section is 16% of σ_1 and in the region up to $\theta_{\mathrm{cross}} = 300$ μrad is 56% of σ_1.

The cross-section of process (10), when the nucleus is excited by strong peripheral nuclear interactions, is less,

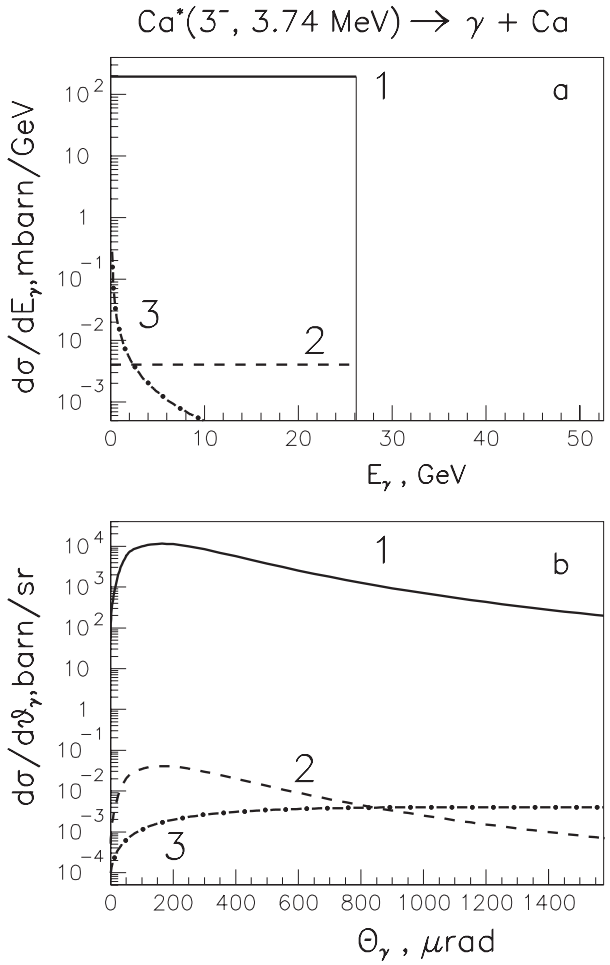

Fig. 4. Comparison of energy (a) and angular (b) distributions of secondary photons for three peripheral processes: (1) nuclear excitation by electrons or positrons in electromagnetic interactions, (2) excitation in strong interaction with $b > 2R_A$, (3) photons from decay $\pi^0 \to 2\gamma$ in process of virtual fusion in AA collisions.

$\sigma_2 = 0.1$ mb, than the process (7), see fig. 4. We calculate this cross-section in eq. (67). We neglect absorption effects in nucleus-nucleus interactions obtaining an upper estimate. We also assumed that the photon angular distribution in the NR system is isotropic. The calculations are for $b > R_A$ with $R_A = 1.2A^{1/3}$ fm for each nucleus.

The distributions of process (2), photon fusion to π^0, was calculated in the same way as our previous work [5] for PbPb collisions. The cross-section of this process is also small, $\sigma_3 = 0.19$ mb, compared with the two-stage cross-section. The energy distribution of photons from π^0 decays in fig. 4a has a peak at $E_\gamma = 0$ because we integrate over all π^0 directions. The angular distribution in fig. 4b has a very different dependence compared to the photon angular distribution of the nuclear radiation.

4 Conclusions

We have presented the energy and angular distributions of secondary photons from nuclear radiation in peripheral ultra-relativistic AA collisions at the LHC. The two-stage process of nuclear excitation by an electron or positron, produced by virtual-photon interactions has a large cross-section, ~ 5 b, along with a specific angular distribution. The secondary γ-radiation at angles ~ 100 μrad and at energies ~ 20 GeV can be measured in the region of TOTEM Roman pots. High-energy γ-radiation in peripheral collisions will be a significant background in the nuclear fragmentation region with an intensity of $\sim 10^6$ photons/s for CaCa collisions at $L \approx 10^{30}$ cm^{-2} s^{-1}.

Secondary γ-radiation from nuclei can be used to monitor the beam intensity, a very difficult problem for nuclear beams. However, it is necessary to determine $R_{\min}$ for nuclear electromagnetic interaction beforehand.

Finally secondary nuclear photons can be a good method for triggering processes (13) or (14) with the meson system produced in the central rapidity region. The full trigger includes a signal in the central rapidity region along with an absence of signals from neutrons and charged nuclear fragments in the nuclear fragmentation region and high-energy secondary photons in the Roman pots.

We are very grateful to L.I. Sarycheva, V.A. Bodyagin, D.E. Lanskoy, I.A. Pshenichnov and V.V. Varlamov for the useful discussions and to N.P. Karpinskaya for the help with the manuscript. We also thank G. Baur, K. Hencken and R. Vogt for helpful comments on our first draft.

References

1. F. Krauss, M. Greiner, G. Soft, Prog. Part. Nucl. Phys. **39**, 503 (1977).
2. G. Baur, K. Hencken, D. Trautmann, J. Phys. G **24**, 1657 (1998).
3. G. Baur, K. Hencken, D. Trautmann, S. Sadovsky, Yu. Kharlov, CMS Note 1998/009, hep-ph/9904361.
4. S. Klein, J. Nystrand, Phys. Rev. C **60**, 014903 (1999).
5. K.A. Chikin *et al.*, Eur. Phys. J. A **8**, 537 (2000).
6. I.A. Pshenichnov *et al.*, Phys. Rev. C **60**, 044901 (1999).
7. I.A. Pshenichnov *et al.*, Phys. Rev. C **57**, 1920 (1998).
8. V. Emel'yanov, A. Khodirov, S. Klein, R.Vogt, LBNL-40398, 1997.
9. J. Nystrand, S. Klein, LBNL-42524, 1998, nucl-ex/9811007.
10. N. Baron, G. Baur, Phys. Rev. D **46**, R3695 (1992).
11. M.J. Rhoades-Brown, J. Weneser, Phys. Rev. A **44**, 330 (1991).
12. M.C. Güclü *et al.*, Phys. Rev. A **51**, 1836 (1995).
13. A. Alscher *et al.*, Phys. Rev. A **55**, 396 (1997).
14. C.A. Bertulani, G. Baur, Phys. Rep. **163**, 299 (1988).
15. H. Meier *et al.*, Eur. Phys. J. C **2**, 741 (1998).
16. S. Jeon, J. Kapusta, A. Chikanian, J. Sandweiss, nucl-th/9806047.
17. K. Hencken, D. Trautmann, G. Baur, nucl-th/9903019.
18. P.M. Endt *et al.*, Nucl. Phys. A **633**, 1 (1998).
19. V.V. Balashov, V.L. Korotkikh, I.V. Moskalenko, *Proceedings of the 21 ICRC, Adelaide*, Vol. **2** (University of Adelaide, 1990) p. 416.
20. S.U. Chung, D.P. Weygand, H.J. Willutzki, Preprint BNL-QGS-02-91.

21. R. Engel *et al.*, Z. Phys. C **74**, 687 (1997).
22. C.G. Roldao, A.A. Natale, Phys. Rev. C **61**, 064907 (2000).
23. W. Kienzle *et al.*, TOTEM, Letter of Intent, CERN/LHCC/ 97-49, 1997.
24. C. Adler, A. Denisov, E. Garcia, M. Mureau, H. Stroebele, S. White, nucl-ex/0008005.
25. I.S. Gulkarov, Fis. Elem. Chast. At Nucl., **19**, 345 (1998).
26. R.J. Glauber, *High Energy Collision Theory. Lectures on Theoretical Physics*, Vol. **1** (Interscience Publ., NY, 1959) p. 315.
27. V.L. Korotkikh, I.P. Lokhtin, Sov. J. Nucl. Phys. **56**, 1110 (1993).
28. K. Goulianos, Comments Nucl. Part. Phys. **17**, 177 (1987).